Flow development over an SD7003 airfoil at different accelerations from rest

Wolfgang Dierl[1,*], Serhiy Yarusevych[2], Rainer Hain[1], Christian J. Kähler[1]

1: Institute of Fluid Mechanics and Aerodynamics, University of the Bundeswehr Munich, Germany
2: Department of Mechanical and Mechatronics Engineering, University of Waterloo, Canada
*Corresponding author: wolfgang.dierl@unibw.de

Keywords: Acceleration, laminar separation bubble, vortex shedding.

ABSTRACT

This work examines the effect of acceleration on the formation of a laminar separation bubble (LSB). The experiments were performed in a water towing tank with an SD7003 airfoil model accelerated from rest to a constant chord Reynolds number. Quantitative flow field measurements were performed using two-component time-resolved Particle Image Velocimetry (PIV) over a range of accelerations. A detailed analysis of the spatio-temporal flow development is conducted focusing on the LSB formation and dynamics. The results provide insight into the mechanism of LSB formation. The associated transient flow development is shown to persist over several convective time units after steady state free-stream velocity is reached, with no significant effect of acceleration on the overall transient duration. However, the acceleration rate has a substantial effect on flow development during the acceleration phase.

1. Introduction

Rapid advancements of applications operating at aerodynamically low Reynolds numbers ($\mathrm{Re}_c \leq 500,000$), like high-altitude, long-endurance unmanned aerial vehicles and micro air vehicles, continues to pose new research challenges. A defining feature for a lifting surface operating at a low Reynolds number is laminar boundary layer separation on the suction side, which leads to a notable degradation in aerodynamic performance and unsteady loading (Lissaman, 1983; Carmichael, 1981), as well as noise emissions (Arcondoulis et al., 2010). After flow separation, a relatively rapid transition to turbulence takes place in the separated shear layer, which often leads to flow reattachment in the mean sense and the formation of a closed, recirculating flow region referred to as a laminar separation bubble (LSB). The transition process is often initiated by the amplification of Tollmien-Schlichting waves upstream of separation, followed by a much stronger growth rate of flow disturbances, primarily driven by a Kelvin-Helmholtz instability in the separated shear layer (Marxen et al., 2013; Michelis et al., 2018). The latter results in shear-layer roll-up and subsequent vortex shedding (Watmuff, 1999; Hain et al., 2009). Downstream of

the reattachment point, a three-dimensional breakup of the vortices occurs (Marxen et al., 2013; Hain et al., 2009). The associated flow development and parametric effects of the angle of attack, Reynolds number, and free-stream turbulence intensity have been considered in a number of previous investigations (Burgmann & Schröder, 2008; Ol et al., 2005; Hain et al., 2009). However, the overwhelming majority of prior studies were conducted under quasi-steady incoming flow conditions. In contrast, the transient flow effects on the LSB have received less attention, despite being encountered in most practical applications.
Recently, there has been increasing interest in the investigation of unsteady flow conditions and their influence on the LSB. The influence of periodic gusts was investigated by numerical simulations (Ohno et al., 2023), and the unsteady LSB on a pitching wing was experimentally characterized (Grille Guerra et al., 2023; Nati et al., 2015). The effect of free-stream acceleration and deceleration between non-zero limiting velocity values was investigated by Ellsworth & Mueller (1991) and Toppings & Yarusevych (2023). The results show that the LSB response to changes in Reynolds number (Re) depends on the rate of acceleration and deceleration. Ellsworth & Mueller (1991) revealed substantial differences for high rates of acceleration and deceleration from the behaviour expected from similar quasi-steady changes. Similar observations have been reported in other studies that considered separating flows on lifting surfaces under unsteady conditions (e.g. Mancini et al., 2015). In contrast to this, Toppings & Yarusevych (2023) showed that the response of an LSB to relatively low rates of acceleration and deceleration follows the expected trends of a quasi-steady change of the inflow conditions. The present work experimentally investigates the initial spatio-temporal formation process of an LSB over an airfoil accelerating from rest to a constant Re. This corresponds to a launch with relatively high acceleration rates, such as a catapult launch of UAVs (Austin, 2010).

2. Experimental setup

All experiments were performed in a water towing tank at the University of the Bundeswehr Munich. The test section is 8 m long, with a cross-section of $0.9 \times 0.9\,\mathrm{m}^2$. The water height during the experiments was 0.75 m. An SD7003 airfoil model with a chord length $c = 250\,\mathrm{mm}$ and a span of 750 mm was employed. The model was positioned vertically and equipped with a brush seal to seal the gap at the floor. To prevent distortions from the water surface and mitigate end effects, a glass end plate was installed, see Fig. 1a. The model was mounted at an angle of attack $\alpha = 6^\circ$ and was accelerated from rest to a constant chord Reynolds number $\mathrm{Re_c}$. Four accelerations *a* were considered. The corresponding non-dimensional acceleration parameter is defined by

$$A_\mathrm{C} = \frac{a \cdot c}{U_\mathrm{final}^2} \tag{1}$$

where U_final is the final, steady state velocity. The considered values and the corresponding towing velocity profiles are shown in Fig. 2.

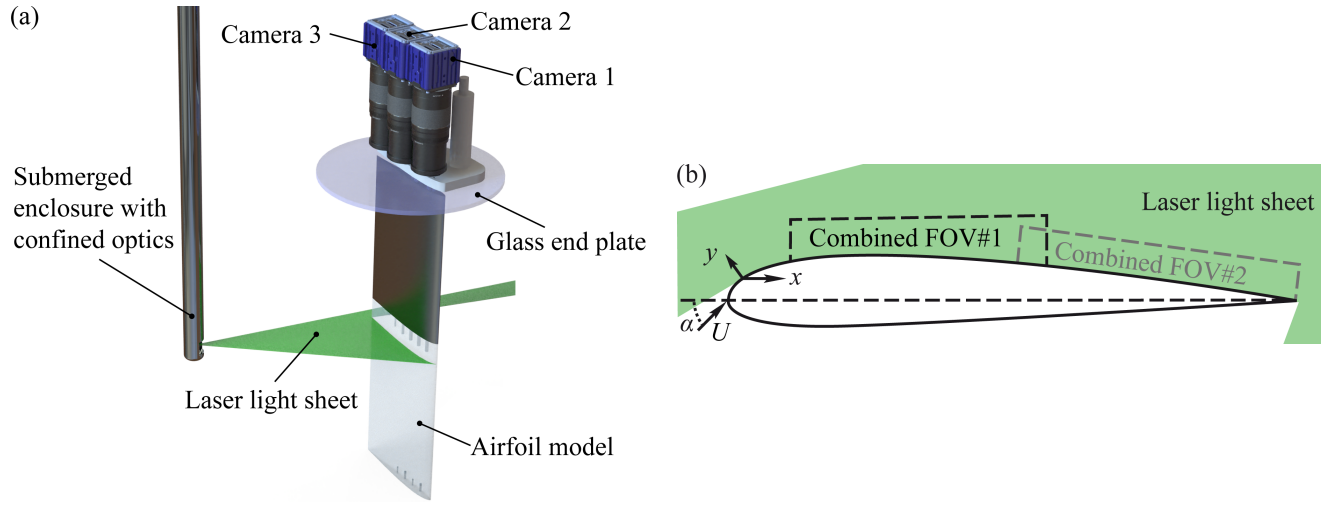

Figure 1. Experimental setup (a) wing model and PIV arrangement (b) Fields of View (FOV) and coordinate system definition.

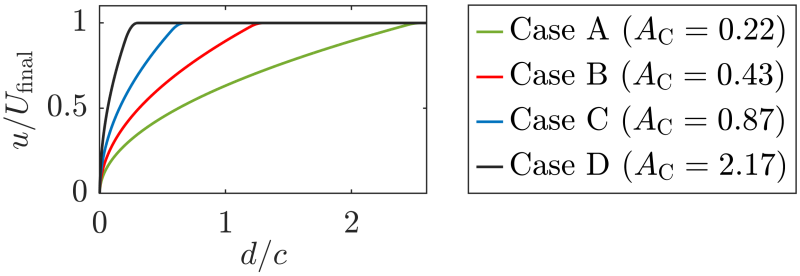

Figure 2. Velocity profiles

Quantitative flow field measurements were performed using two-component time-resolved Particle Image Velocimetry (PIV) in a setup illustrated in Fig. 1a. The water in the tank was seeded with 10 µm hollow glass spheres with a specific gravity of 1.1. The flow was illuminated by a Photonics DM150-532 DH Nd:YAG double-pulse laser. The laser sheet was formed using optics confined within a submerged enclosure connected to the carriage of the towing tank. Particle images were acquired by three cameras (LaVision Imager sCMOS) at 55 Hz in double-frame mode. Each camera was equipped with a Zeiss 100 mm fixed focal-length lens set to a numerical aperture of $f_{\#} = 4$. The camera sensors were cropped to $2560 \times 967\,\text{px}^2$ each. The combined field of view (cFOV) at measurement position #1 and #2 (Fig. 1b) from all three cameras was $18 \times 145\,\text{mm}^2$, with a magnification factor of 0.31. The vector fields were computed with LaVision DaVis 10 software using multi-pass cross-correlation with image deformation. A final interrogation window size of $24 \times 24\,\text{px}^2$ with an overlap of 75 % was used, resulting in a vector pitch of 0.13 mm for cFOV #1 and #2. Table 1 presents essential PIV parameters. All the results are presented in the wall-attached coordinates (Fig. 1b).

A magnet band sensor (MBS) was used to measure the position of the carriage. The MBS data were recorded at 100 kHz simultaneously with the Q-switch signal from the laser, allowing to establish

Table 1. PIV parameters

Parameters	
Light source	Photonics DM150-532 DH Nd:YAG
Light sheet thickness	2 mm
Laser pulse separation	1.1 ms
Seeding	LaVision 10 µm hollow glass spheres
Seeding specific gravity	1.1
Cameras	$3\times$ LaVision Imager sCMOS
Sensor size	$2560 \times 967\,\mathrm{px}^2$
Combined field of view	$18 \times 145\,\mathrm{mm}^2$
Lens focal length	100 mm
Aperture $f_\#$	4
Magnification factor	0.31
Sampling frequency	55 Hz
Free-stream particle image displacement	17 px
Final interrogation window size	$24 \times 24\,\mathrm{px}^2$

the temporal relation between the measured airfoil motion and velocity fields.

Ten independent test runs, each yielding 400 velocity fields, were conducted per case (Fig. 2). The distance travelled over which velocity measurements were conducted for each run was 3.25 m or $13 \cdot c$. PIV measurements were performed for cFOV #1 and the runs were repeated to facilitate measurements in cFOV #2 (Fig. 1b). PIV measurements were also performed to characterize the perturbations in the tank induced by the model motion. The time separation between each run was set to at least 300 s to minimize any adverse influence of residual perturbations from the previous run. Based on a reference velocity of $u_{\mathrm{ref}} = 240\,\mathrm{mm/s}$ ($\widehat{=}\,\mathrm{Re_c} = 60.000$), this ensured that the mean residual flow velocity u_{m} and turbulence intensity level in the towing tank dropped below 1.2 % and 0.05 %, respectively.

3. Results

The formation of the LSB for Case C (velocity profile see Fig. 2) is depicted in Figure 3, which illustrates the overall flow development on the suction side of the airfoil using spanwise vorticity contours. The sequences of consecutive time frames are grouped into three time intervals, corresponding to the three phases of flow development. The first frame corresponds to $t = 1.09\,\mathrm{s}$ from the onset of airfoil motion. At this time the acceleration phase is about to finish, followed by the second frame wherein the model moves at a constant speed. During the first phase a laminar boundary layer forms over the wing. Due to the acceleration the boundary layer is stable. How-

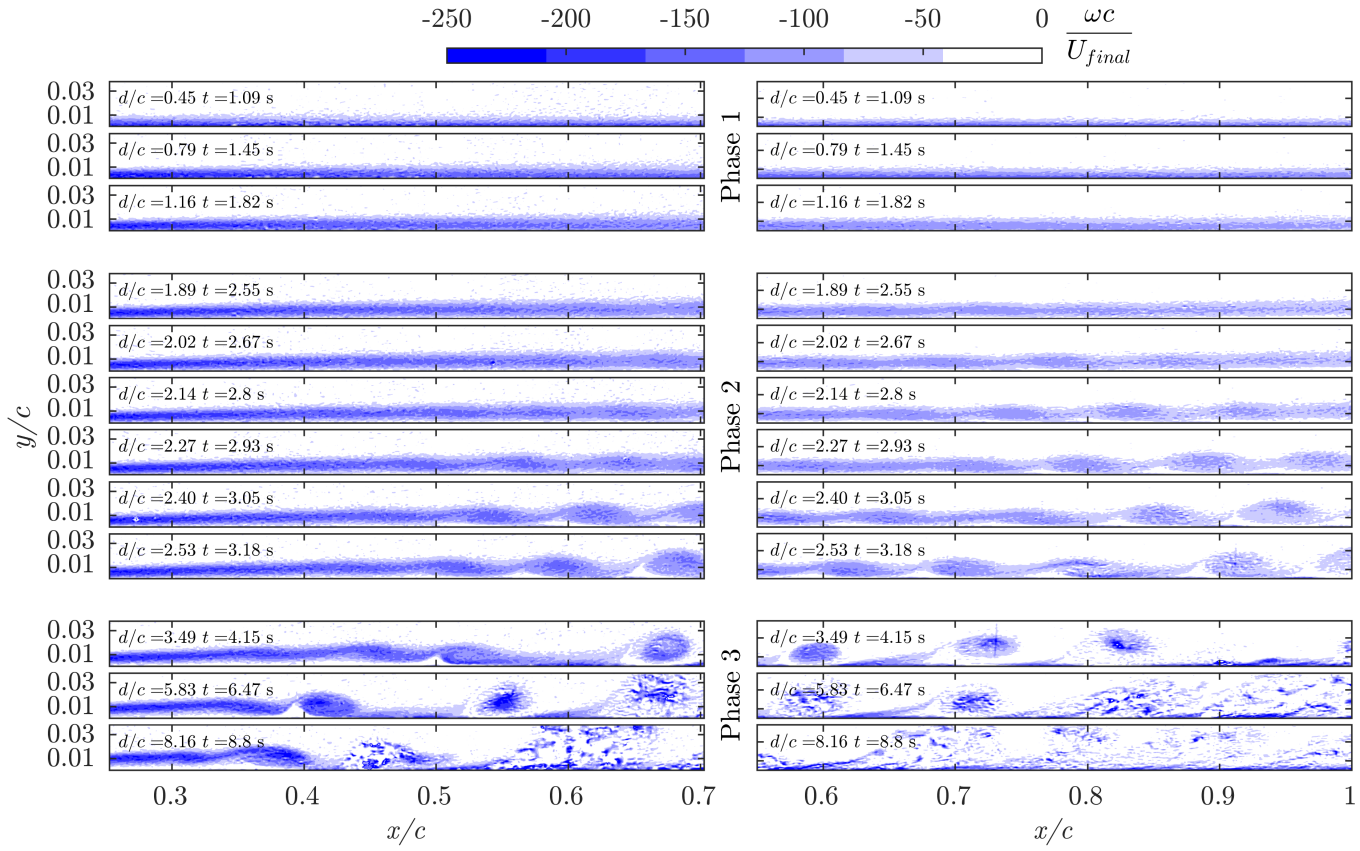

Figure 3. Transient flow development for Case C illustrated by spanwise vorticity contours.

ever the growth of the boundary layer thickness with time can be observed. During the second phase, the boundary layer thickness is quite stationary, however, notable perturbations appear in the boundary layer and are amplified, resulting in a simultaneous formation of an oscillatory vorticity pattern in a region located primarily within the second field of view. The onset of disturbances moves upstream with time. Finally, during the third phase, a distinct shear layer roll-up can be identified, and its location moves continuously towards the leading edge, eventually settling on a quasi-steady LSB dynamics.

Figure 4 offers another perspective on the spatio-temporal flow development. It presents contours of local boundary layer displacement thickness δ^* computed based on the integration of the wall-tangential velocity component over the vertical extent of the field of view, with the local instantaneous edge velocity taken as the reference. The results are plotted versus the relative distance travelled by the wing d/c, with the distance at which the final velocity is reached marked by the black dotted line. It can be seen that acceleration from rest results in significant changes in the flow, which take several convective time units to reach quasi-steady state after the final wing velocity is reached. In particular, a continuous growth of δ^* with respect to d/c can be seen at all x/c locations, saturating at approximately $d/c = 8$. Although the distance travelled during the acceleration phase for Case A and Case D differs by a factor of 8 ($2.5c$ vs. $0.3c$), no significant difference can

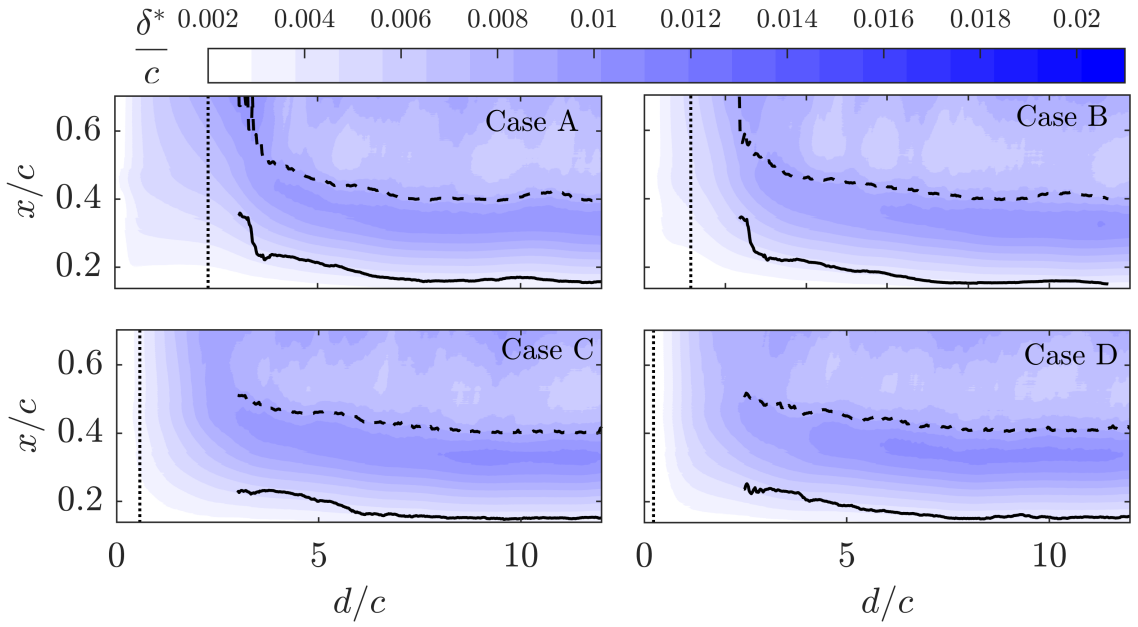

Figure 4. Spatio-temporal evolution of displacement thickness for all cases in cFOV#1. With —— indicating the separation point, - - - the reattachment point and ····· end of acceleration.

be seen in the time it takes for the displacement thickness to reach quasi-steady values. Based on a moving window average over 30 frames, an estimate of separation and reattachment locations is provided by the solid and dashed lines, respectively. They show an upstream movement of an LSB, which moves into cFOV#1 at $d/c = 2.4$, corresponding to frame five of phase two in Fig. 3. Furthermore, the length of the LSB remains relatively constant during the upstream movement, as the distance between the solid and dashed line does not change appreciably beyond $d/c = 4$. The associated periodic shedding of shear-layer structures is reflected in periodic fluctuations in the computed δ^* in Fig. 4.

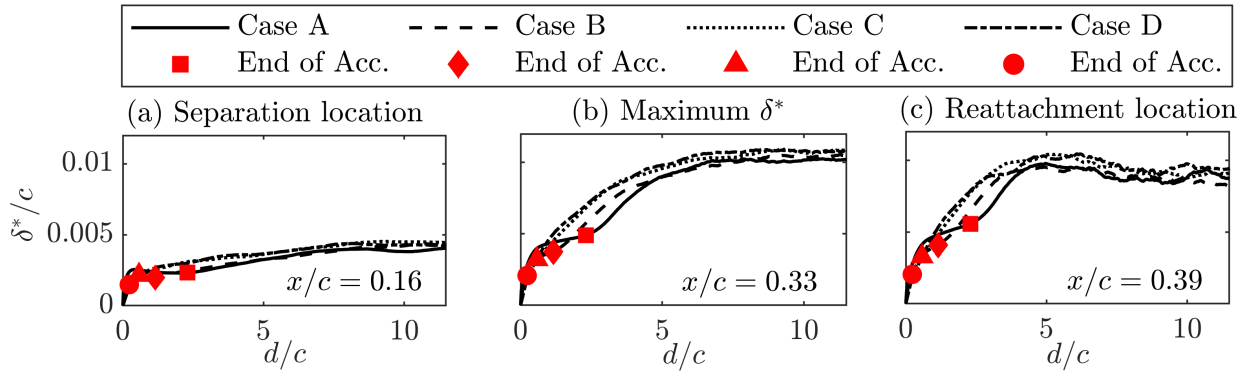

Figure 5. Variation of displacement thickness computed at three chord positions corresponding to (a) separation location, (b) location of maximum δ^*, and (c) reattachment locations in the quasi-steady LSB.

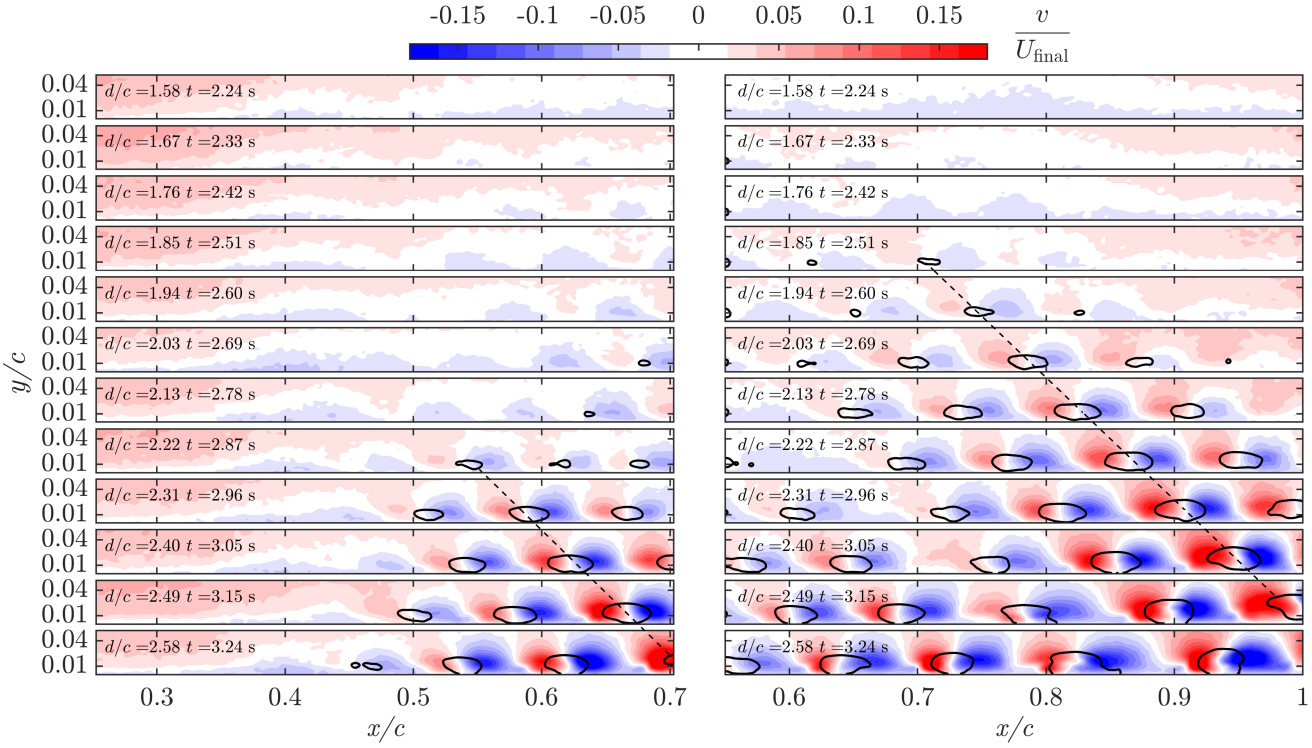

Figure 6. Process of initial vortex formation for Case C illustrated by the non-dimensional wall-normal velocity component. Solid black line contours correspond to $\lambda_2 = -70$.

The effect of flow acceleration is explored in Fig. 5, which presents δ^* computed at three x/c locations for all the accelerations investigated. The chosen x/c locations correspond to the separation point, the point of maximum bubble height, and the reattachment point of the LSB in final quasi-steady state. While notable differences are observed at the earlier stages of flow development, the results indicate that significant changes take place in the flow field after the acceleration phase, and the overall transient takes approximately eight convective times for all accelerations investigated. This agrees with the transient duration for an LSB due to changes in controlled perturbations (Yarusevych et al. (2009)), suggesting that the transient dynamics is associated with the development of LSB. At the earlier stages of flow development, Cases C and D show a continuous growth in δ^* with subsequent saturation to a steady state value. In contrast, an intermediate plateau is reached in δ^* for Cases A and B during the second half of the acceleration phase, and continuous growth in displacement thickness is reestablished when the final wing velocity is reached. A detailed analysis of the results revealed that the observed differences in the flow development during the initial phase of acceleration are related to the differences in the onset and development of shear-layer perturbations.

To evaluate the initial LSB formation in detail, Fig. 6 illustrates the onset of vortex formation over the airfoil by a sequence of consecutive time frames, spaced by $5/55\,\text{s}$, with the first frame corresponding to $t = 2.24\,\text{s}$ from the onset of airfoil motion. The results reveal the appearance of

periodic undulations in the shear-layer that develop into distinct periodic shedding of vortices at later times, similar to the Kelvin-Helmholtz instability driven vortex shedding in a quasi-steady LSB (e.g. Watmuff, 1999). However, low amplitude perturbations that can be inferred from the waviness of the shear-layer in the first flow field of the sequence appear to grow both in space and time. The distinct convective amplification can be seen by tracing the same structures in subsequent images, some of which are connected by dashed lines in Fig. 6. Also, a notable increase in fluctuation amplitude can be observed at a given x/c location, for example at $x/c = 0.6$. This may indicate that the initial stage of transition is governed by a combination of convective and global instability mechanisms. Progressively, the convective instability mechanism appears to take over, and a typical spatial amplification is observed in the last frames of the sequence.

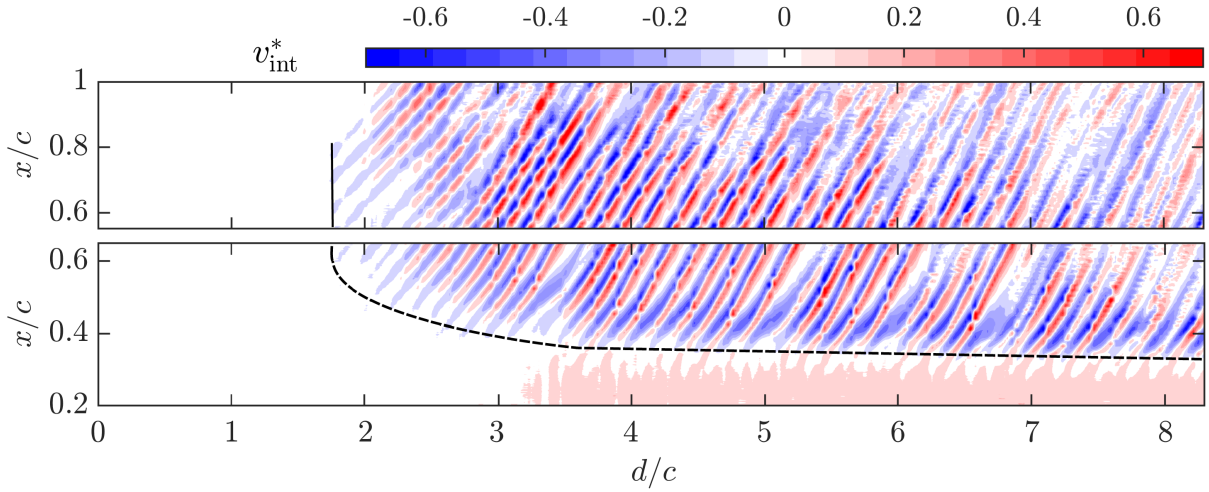

Figure 7. Integrated wall-normal velocity contours. Simultaneous appearance of detectable perturbations of comparable amplitude —— and progressive upstream movement of the roll-up location - - -.

Figure 7 provides a more quantitative perspective on the spatio-temporal development of the vortex formation process. The integrated wall-normal velocity from surface up to $y/c = 0.03$ is plotted over d/c, with vortex shedding signified by alternating positive and negative convective ridges. The results show a nearly simultaneous appearance of detectable perturbations of comparable amplitude, marked by the solid black line. This is followed by a progressive upstream movement of the roll-up location, marked by the dashed line. Initially, the upstream movement of the roll-up locations takes place at a relatively high rate ($0.26c\,\mathrm{s}^{-1}$), which reduces gradually as a quasi-steady shedding is established at $d/c \sim 8$. The estimated drift velocity of the vortices is $U_{\mathrm{drift}} = 0.62 \cdot U_{\mathrm{final}}$, which agrees well with $U_{\mathrm{drift}} = 0.65 \cdot U_{\infty}$ reported for a quasi-steady LSB by Pauley et al. (1990). In order to characterize the vortex shedding frequency during LSB formation, a wavelet analysis is performed based on a complex Morlet wavelet (Studer et al., 2006). The results are show in Fig. 8, along with a reference spectrogram obtained in a quasi-steady LSB. The spectrogram shows a dominant peak at 5.7 Hz, corresponding to a chord-based Strouhal number of 5.7. The results show that, despite significant transient changes in vortex shedding reflected in the variation of the

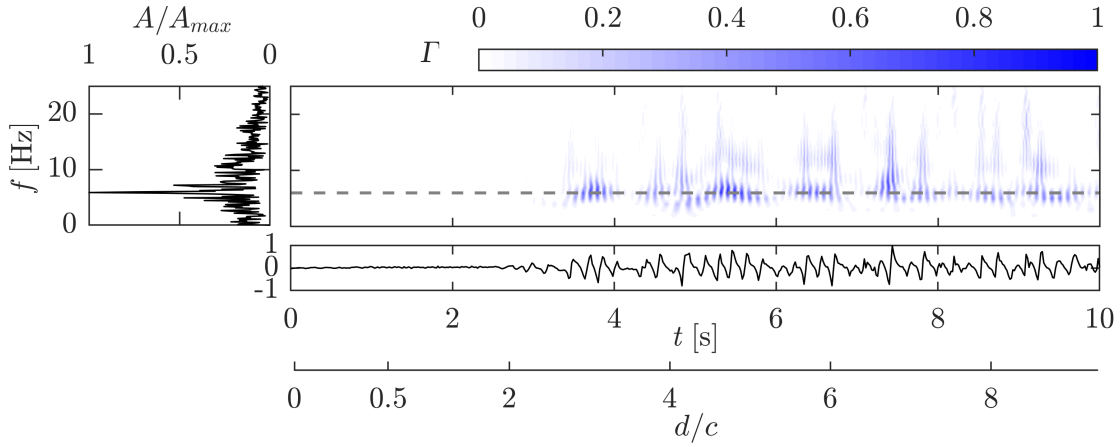

Figure 8. Normalized wavelet coefficient (Γ) contours from wall-normal velocity fluctuation. Extracted normalized fluctuation signal shown on the bottom with corresponding Fourier analysis on the left.

magnitude of the wavelet coefficients, the shedding frequency remains relatively constant. Note that the observed temporal fluctuations in the shedding frequency are representative of those seen in a quasi-steady LSB, similar to the findings of Kurelek et al. (2019). The estimated shedding frequency is in general agreement with the parametric correlation provided in Boutilier & Yarusevych (2012), but is lower than that measured by Burgmann & Schröder (2008) for the same airfoil profile at matching operating conditions. The latter can be attributed to a notably higher level of background perturbations in the experiments of Burgmann & Schröder (2008), which also results in a smaller LSB.

4. Conclusions

The present study examined the transient flow development on an airfoil accelerated to a constant velocity from rest. The transient process consists of three distinct phases. During the first phase, laminar boundary layer develops on the suction side, and the effect of acceleration is largely confined to this phase. This is followed by nearly simultaneous formation of cat's-eye structures over a region of the flow field in phase two. The observed growth of the associated velocity perturbations occurs both in time and space, ascribed to the presence of absolute and convective instabilities. The shear layer roll-up location progressively moves upstream in phase three, as the LSB settles on quasi-steady shedding. The wavelet analysis reveals that the shedding frequency remains nearly constant from the onset of shedding to quasi-steady LSB.

5. Acknowledgement

The authors gratefully acknowledge the financial support of the German Research Foundation (DFG) for this project (Analysis of the transition process around laminar separation bubbles (LSB's) in a towing tank using time-resolved 3D particle tracking techniques, project number 422177304).

References

Arcondoulis, E. J. G., Doolan, C. J., Zander, A. C., & Brooks, L. A. (2010). A review of trailing edge noise generated by airfoils at low to moderate Reynolds number. *Acoustics Australia*, *38*(3), 129–133.

Austin, R. (2010). *Unmanned Aircraft Systems: UAVS Design, Development and Deployment*. Wiley.

Boutilier, M. S. H., & Yarusevych, S. (2012). Parametric study of separation and transition characteristics over an airfoil at low Reynolds numbers. *Experiments in Fluids*, *52*(6), 1491–1506. doi: 10.1007/s00348-012-1270-z

Burgmann, S., & Schröder, W. (2008). Investigation of the vortex induced unsteadiness of a separation bubble via time-resolved and scanning PIV measurements. *Experiments in Fluids*, *45*(4), 675–691. doi: 10.1007/s00348-008-0548-7

Carmichael, B. (1981). Low Reynolds number airfoil survey, volume 1. *NASA Contractor Report*, *165803*.

Ellsworth, R. H., & Mueller, T. J. (1991). Airfoil boundary layer measurements at low Re in an accelerating flow from a nonzero velocity. *Experiments in Fluids*, *11*(6), 368–374. doi: 10.1007/BF00211791

Grille Guerra, A., Mertens, C., Little, J., & van Oudheusden, B. (2023). Experimental characterization of an unsteady laminar separation bubble on a pitching wing. *Experiments in Fluids*, *64*(1), 16. doi: 10.1007/s00348-022-03564-w

Hain, R., Kähler, C. J., & Radespiel, R. (2009). Dynamics of laminar separation bubbles at low-Reynolds-number aerofoils. *Journal of Fluid Mechanics*, *630*, 129–153. doi: 10.1017/S0022112009006661

Kurelek, J. W., Yarusevych, S., & Kotsonis, M. (2019, Jun). Vortex merging in a laminar separation bubble under natural and forced conditions. *Physical Review Fluids*, *4*, 063903. Retrieved from `https://link.aps.org/doi/10.1103/PhysRevFluids.4.063903` doi: 10.1103/PhysRevFluids.4.063903

Lissaman, P. B. S. (1983). Low-Reynolds-Number Airfoils. *Annual Review of Fluid Mechanics*, *15*(1), 223–239. doi: 10.1146/annurev.fl.15.010183.001255

Mancini, P., Manar, F., Granlund, K., Ol, M. V., & Jones, A. R. (2015). Unsteady aerodynamic characteristics of a translating rigid wing at low Reynolds number. *Physics of Fluids*, *27*(12), 123102. doi: 10.1063/1.4936396

Marxen, O., Lang, M., & Rist, U. (2013). Vortex formation and vortex breakup in a laminar separation bubble. *Journal of Fluid Mechanics*, *728*, 58–90.

Michelis, T., Yarusevych, S., & Kotsonis, M. (2018). On the origin of spanwise vortex deformations in laminar separation bubbles. *Journal of Fluid Mechanics*, *841*, 81—108. doi: 10.1017/jfm.2018.91

Nati, A., de Kat, R., Scarano, F., & van Oudheusden, B. W. (2015). Dynamic pitching effect on a laminar separation bubble. *Experiments in Fluids*, *56*(9), 1. doi: 10.1007/s00348-015-2031-6

Ohno, D., Greiner, M., Müller, J., & Rist, U. (2023). Numerical Investigations of Laminar Separation Bubbles Under the Influence of Periodic Gusts. *AIAA Journal*, *61*(6), 2486-2499. doi: 10.2514/1.J062510

Ol, M. V., McCauliffe, B., Hanff, E., Scholz, U., & Kaehler, C. J. (2005). Comparison of Laminar Separation Bubble Measurements on a Low Reynolds Number Airfoil in Three Facilities. In *35th aiaa fluid dynamics conference and exhibit* (p. 483). Reston, Virigina: American Institute of Aeronautics and Astronautics. doi: 10.2514/6.2005-5149

Pauley, L. L., Moin, P., & Reynolds, W. C. (1990). The structure of two-dimensional separation. *Journal of Fluid Mechanics*, *220*, 397–411. doi: 10.1017/S0022112090003317

Studer, G., Arnal, G., Houdeville, R., & Seraudie, A. (2006). Laminar–turbulent transition in oscillating boundary layer: experimental and numerical analysis using continuous wavelet transform. *Experiments in Fluids*, *41*, 685–698. doi: 10.1007/s00348-006-0190-1

Toppings, C., & Yarusevych, S. (2023). Transient dynamics of laminar separation bubble formation and bursting. *Experiments in Fluids*, *64*, 57. doi: https://doi.org/10.1007/s00348-023-03590-2

Watmuff, J. H. (1999). Evolution of a wave packet into vortex loops in a laminar separation bubble. *Journal of Fluid Mechanics*, *397*, 119–169. doi: 10.1017/S0022112099006138

Yarusevych, S., Sullivan, P. E., & Kawall, J. G. (2009). On vortex shedding from an airfoil in low-Reynolds-number flows. *Journal of Fluid Mechanics*, *632*, 245–271. doi: 10.1017/S0022112009007058